Early temporal dynamics of cellular responses to SARS-CoV-2

Arinjay Banerjee[1,2], Patrick Budylowski[3], Daniel Richard[4], Hassaan Maan[5,6], Jennifer A. Aguiar[7], Nader El-Sayes[2], Michael R. D'Agostino[2], Benjamin J.-M. Tremblay[7], Sam Afkhami[2], Mehran Karimzadeh[5,6,8], Lily Yip[9], Mario Ostrowski[10], Jeremy A. Hirota[2,11], Robert Kozak[9,12], Terence D. Capellini[4], Matthew S. Miller[2,13], Andrew G. McArthur[2,13], Bo Wang[5,6,8], Andrew C. Doxey[7,11], Samira Mubareka[9,12] and Karen Mossman[1,2,*]

[1]Department of Pathology and Molecular Medicine, McMaster University; Hamilton, ON, Canada.

[2]Michael G. DeGroote Institute for Infectious Disease Research, McMaster University; Hamilton, ON, Canada.

[3]Institute of Medical Science, University of Toronto, Toronto, ON, Canada

[4]Department of Human Evolutionary Biology, Harvard University, Cambridge, MA, USA.

[5]Vector Institute for Artificial Intelligence, Toronto, ON, Canada

[6]Peter Munk Cardiac Centre, University Health Network, Toronto, ON, Canada.

[7]Department of Biology, University of Waterloo; Waterloo, Ontario, N2L 3G1; Canada

[8]Department of Medical Biophysics, University of Toronto, ON, Canada

[9]Sunnybrook Research Institute, Toronto, ON, Canada

[10]Department of Medicine, University of Toronto, Toronto, ON, Canada

[11]Division of Respirology, Department of Medicine, McMaster University, Hamilton, ON, Canada.

[12]Department of Laboratory Medicine and Pathobiology, University of Toronto, Toronto, ON, Canada.

[13]Department of Biochemistry and Biomedical Sciences, McMaster University, Hamilton, ON, Canada.

*Corresponding author:

Dr. Karen Mossman

Email: mossk@mcmaster.ca

Classification: Biological Sciences; Microbiology

Keywords: SARS-CoV-2, transcription, interferon, ISGs, coronavirus

Author contributions: A.B., D.R., H.M., A.G.M. and J.A.A. designed the study; A.B., P.B., N.E-.S., M.R.D., S.A. and L.Y. performed research; A.B., D.R., H.M., J.A.A, N.E-.S., B.J.-M.T., and M.K. analyzed the data; J.A.H. and M.S.M. provided reagents; A.B., M.O., J.A.H., R.K., T.C., M.S.M., A.G.M, A.C.D., S.M. and K.M. provided funding and supervised the study; A.B., D.R., H.M., N.E-.S., J.A.A. and A.G.M. wrote the manuscript. All authors reviewed the manuscript.

Abstract

Two highly pathogenic human coronaviruses that cause severe acute respiratory syndrome (SARS) and Middle East respiratory syndrome (MERS) have evolved proteins that can inhibit host antiviral responses, likely contributing to disease progression and high case-fatality rates. SARS-CoV-2 emerged in December 2019 resulting in a global pandemic. Recent studies have shown that SARS-CoV-2 is unable to induce a robust type I interferon (IFN) response in human cells, leading to speculation about the ability of SARS-CoV-2 to inhibit innate antiviral responses. However, innate antiviral responses are dynamic in nature and gene expression levels rapidly change within minutes to hours. In this study, we have performed a time series RNA-seq and selective immunoblot analysis of SARS-CoV-2 infected lung (Calu-3) cells to characterize early virus-host processes. SARS-CoV-2 infection upregulated transcripts for type I IFNs and interferon stimulated genes (ISGs) after 12 hours. Furthermore, we analyzed the ability of SARS-CoV-2 to inhibit type I IFN production and downstream antiviral signaling in human cells. Using exogenous stimuli, we discovered that SARS-CoV-2 is unable to modulate *IFNβ* production and downstream expression of ISGs, such as *IRF7* and *IFIT1*. Thus, data from our study indicate that SARS-CoV-2 may have evolved additional mechanisms, such as masking of viral nucleic acid sensing by host cells to mount a dampened innate antiviral response. Further studies are required to fully identify the range of immune-modulatory strategies of SARS-CoV-2.

Significance

Highly pathogenic coronaviruses that cause SARS and MERS have evolved proteins to shutdown antiviral responses. The emergence and rapid spread of SARS-CoV-2, along with its relatively low case-fatality rate have led to speculation about its ability to modulate antiviral

responses. We show that SARS-CoV-2 is unable to block antiviral responses that are mounted by exogenous stimuli. Data from our study provide promising support for the use of recombinant type I IFN as combination therapy to treat COVID-19 patients. Furthermore, our data also suggest that the inability of SARS-CoV-2 to efficiently modulate antiviral responses may be associated with its low case-fatality rate compared to other pathogenic CoVs that cause SARS and MERS.

Main Text

Introduction

Severe acute respiratory syndrome coronavirus 2 (SARS-CoV-2) emerged in December 2019 to cause a global pandemic of coronavirus disease 2019 (COVID-19) (1). SARS-CoV-2 causes a respiratory infection with acute respiratory distress syndrome (ARDS) in severe cases. Innate antiviral responses, which include type I interferons (IFNs) are the first line of defense after a virus enters a cell (2). Cellular pattern recognition receptors (PRRs) recognize viral nucleic acids and activate key cellular kinases, such as inhibitor of nuclear factor kappa-B kinase subunit epsilon (IKKε) and TANK-binding kinase 1 (TBK1). These kinases activate transcription factors, such as interferon regulatory factor 3 (IRF3) to stimulate downstream production of type I IFNs (3).

To counteract host antiviral responses, viruses encode proteins that can modulate type I IFN production and signaling (4, 5). Emerging pathogenic human coronaviruses, such as SARS-CoV and Middle East respiratory syndrome (MERS)-CoV have evolved multiple proteins that can inhibit type I IFN responses in human cells (6-10). Thus, to better understand SARS-CoV-2 pathogenesis, it is critical to identify the early dynamic interactions of SARS-CoV-2 and the type I IFN response.

Data from *in vitro* and *in vivo* work have demonstrated the lack of induction of type I IFN responses following SARS-CoV-2 infection (11). Interestingly, on the contrary, emerging data from patients with mild and moderate cases of COVID-19 have demonstrated the presence of type I IFN (12, 13). Thus, the inability to mount an effective IFN response to SARS-CoV-2 may also be associated with underlying host factors, along with the duration and extent of viral infection. Furthermore, it is unclear if SARS-CoV-2 is unable to stimulate a type I IFN response or actively suppresses the response after initiating it in infected cells.

In this study, we have identified global early transcriptional responses that are initiated during SARS-CoV-2 infection of human lung epithelial (Calu-3) cells at 0, 1, 2, 3, 6, and 12 hours post infection. SARS-CoV-2 infected cells mounted a type I IFN response between 6 and 12 hours post infection (hpi) and the degree of this response correlated with virus replication and transcription. However, a high dose infection of SARS-CoV-2 is unable to modulate poly (I:C)-induced IFNβ production and signaling. Furthermore, SARS-CoV-2 is unable to modulate interferon stimulated gene (ISG) expression in response to exogenous IFNβ. Our study provides insights into early host responses that are generated on infection with SARS-CoV-2 and the inability of the virus to efficiently modulate these responses, which may explain the low case-fatality rate of COVID-19. Furthermore, it is likely that comorbidities and deficiencies in type I IFN responses are associated with severe outcomes in COVID-19 patients. In summary, our data indicate that SARS-CoV-2 is inefficient in modulating type I IFN production and signaling when cells are exogenously stimulated. Further investigations into the ability of SARS-CoV-2 to mask its nucleic acid pathogen associated molecular pattern (PAMP) from cellular PRRs to generate a dampened innate antiviral response is warranted.

Results

SARS-CoV-2 replication proceeds in a directional manner. The replication cycle of CoVs is complex and involves the generation of sub-genomic RNA molecules, which in turn code for mRNA that are translated into proteins (14, 15). To determine SARS-CoV-2 replication kinetics in human cells using RNA-seq, we infected human lung epithelial cells (Calu-3) at a multiplicity of infection (MOI) of 2. One hour post incubation, virus inoculum was replaced with cell growth media and the clock was set to zero hours. We extracted and sequenced poly-A enriched RNA at 0, 1, 2, 3, 6 and 12 hours post infection (hpi). SARS-CoV-2 genome, sub-genomic RNA and transcripts were detected in infected samples; viral transcript expression clustered based on post-infection time using PCA (*SI Appendix,* Fig. S1). From our RNA-seq analysis, we were able to detect high levels of expression of SARS-CoV-2 structural and accessory genes at the 3' end of the genome as early as 0 hpi (Fig. 1A). Significant expression of *ORF1ab*, relative to 0 hpi was detected at 6 hpi (Fig. 1A). SARS-CoV-2 nucleocapsid (*N*) gene was highly expressed relative to other genes as early as 0 hpi (Fig 1B), with relative expression significantly increasing over time (p = 1.4e-16). The absolute expression of other genes increased over time with levels of *N* > *M* > *ORF10* > *S* > *ORF1ab* > *ORF7a* > *ORF8* > *ORF3a* > *ORF6* > *E* > *ORF7b* > *ORF1a* at 12 hpi (Fig. 1B; *SI Appendix*, Table S1).

SARS-CoV-2 induces a mild type I IFN response. We analyzed the early host response mounted by Calu-3 cells that were infected with SARS-CoV-2. Gene expression levels in these cells clustered based on time-points via PCA (*SI Appendix*, Fig. S2). One hundred and twenty-four genes were significantly (FDR-adjusted $p < 0.05$) differentially expressed in infected cells, relative to mock infected cells in at least one time point post infection (absolute $\log_2$ fold-change > 1) (Fig. 1D; *SI Appendix*, Table S2 and Fig. S3). The extent of antiviral gene expression at 12

hpi correlated with an increase in viral transcripts (*SI Appendix*, Fig. S3). Interestingly, at early time points of 2 and 3 hpi, pathway enrichment analysis revealed numerous cellular processes that were significantly downregulated in SARS-CoV-2 infected cells, relative to mock infected cells (FDR-adjusted $p < 0.05$). These processes included RNA splicing, apoptosis, ATP synthesis, and viral and host translation, while genes associated with viral processes, cell adhesion and double-stranded RNA binding were upregulated in infected cells relative to mock infected cells (Fig. 1C and *SI Appendix*, Figs. S4 and S5, Table S3). Cellular pathways associated with type I IFN production and signaling, along with OAS/TRAF-mediated antiviral responses were upregulated at 12 hpi (Figs. 1C and 1D). Consistent with other reports, transcript levels for *IFNβ1* and *IFNλ1* were significantly upregulated at 12 hpi with SARS-CoV-2 at a high MOI of 2 (Fig. 1E) (11). Transcript levels of *IFNλ2* and *IFNλ3* also increased at 6 and 12 hpi, but the levels did not reach significance relative to mock infected cells at these time points (Fig. 1E). At least 19 well-studied antiviral ISGs were upregulated in infected cells, relative to mock infected cells at 12 hpi, including interferon induced protein with tetratricopeptide repeats 1 (*IFIT1*), interferon regulatory factor 7 (*IRF7*), 2'-5-oligoadenylate synthetase 2 (*OAS2*) and MX dynamin GTPase 1 (*MX1*) (Fig. 1F and *SI Appendix*, Fig. S6 and Table S2). Genes associated with structural molecule activity, cell adhesion and exocytosis were downregulated in SARS-CoV-2 infected cells, relative to uninfected cells at 12 hpi (*SI Appendix*, Fig. S5).

SARS-CoV-2 is unable to modulate type I IFN gene expression induced by an exogenous stimulus. Coronaviruses, such as those that cause SARS and MERS have evolved multiple proteins that can modulate type I IFN expression (7-10, 16, 17). To confirm that SARS-CoV-2 infection is sufficient to induce type I IFN and ISG responses in Calu-3 cells, we infected the

cells with SARS-CoV-2 and assessed transcript levels of *IFNβ*, *IRF7* and *IFIT1* by quantitative polymerase chain reaction (qPCR). *IFNβ* induction was observed 12 hpi in SARS-CoV-2 infected cells, relative to mock-infected cells (Fig. 2A). Consistent with the upregulation of *IFNβ* transcripts in SARS-CoV-2 infected cells, transcript levels for ISGs, such as *IRF7* and *IFIT1* were also upregulated 12 hpi (Figs. 2B and 2C).

Next, to identify if SARS-CoV-2 is able to modulate type I IFN responses mounted against an exogenous stimulus, we infected Calu-3 cells with SARS-CoV-2 for 12 hours at a MOI of 2 and stimulated these cells with exogenous double-stranded RNA [poly(I:C)] for 6 hours. We measured the levels of *IFNβ* transcripts in these cells by qPCR. Poly(I:C) transfection alone induced significantly higher levels of *IFNβ* transcripts relative to mock transfected cells (Fig. 2D). Similar to that shown in Fig. 2A, SARS-CoV-2 infection alone also induced high levels of *IFNβ* transcripts relative to mock infected cells (Fig. 2D). However, SARS-CoV-2 infection-induced levels of *IFNβ* transcripts were significantly lower compared to both poly(I:C) transfected cells and SARS-CoV-2 infected + poly(I:C) transfected cells. Interestingly, there was no significant difference in *IFNβ* transcript levels between poly(I:C) transfected and SARS-CoV-2 infected + poly(I:C) transfected cells (Fig. 2D). In fact, there was an increasing trend in *IFNβ* transcript levels in SARS-CoV-2 infected + poly(I:C) transfected cells relative to cells that were transfected with poly(I:C) alone; however, the data were not significant at this time point.

To support our observations with *IFNβ* transcripts in SARS-CoV-2 infected and/or poly(I:C) transfected cells, we also quantified the levels of ISG transcripts, such as *IRF7* and *IFIT1* in these cells. Poly(I:C) transfection alone induced significantly higher levels of *IRF7* and *IFIT1* transcripts relative to mock transfected cells (Figs. 2E and 2F). Similar to that shown in Figs. 2B and 2C, SARS-CoV-2 alone also induced high levels of *IRF7* and *IFIT1* transcripts

relative to mock infected cells (Figs. 2E and 2F). However, SARS-CoV-2 infection-induced levels of *IRF7* and *IFIT1* transcripts were significantly lower compared to both poly(I:C) transfected cells and SARS-CoV-2 infected + poly(I:C) transfected cells. Notably, *IRF7* and *IFIT1* transcript levels in SARS-CoV-2 infected + poly(I:C) transfected cells were significantly higher than levels in cells that were transfected with poly(I:C) alone (Figs. 2E and 2F).

To corroborate our gene expression studies, we repeated our experiments and performed immunoblots for SARS-CoV-2 N, IFIT1 and glyceraldehyde 3-phosphate dehydrogenase (GAPDH). Poly(I:C) transfection induced low levels of IFIT1 in Calu-3 cells, while SARS-CoV-2 infection alone was unable to induce detectable levels of IFIT1 in our immunoblots (Fig. 2G). SARS-CoV-2 infection + poly(I:C) transfection also induced low, but detectable levels of IFIT1 (Fig. 2G). We confirmed SARS-CoV-2 infection in these cells by detecting N protein in the samples (Fig. 2G).

SARS-CoV-2 is unable to modulate type I IFN signaling. SARS-CoV and MERS-CoV proteins can also modulate downstream IFN signaling to restrict the production of ISGs (6). To determine if SARS-CoV-2 can modulate type I IFN signaling in response to exogenous IFNβ treatment, we infected Calu-3 cells for 12 hours at a MOI of 2 and stimulated these cells with recombinant human IFNβ for 6 hours. We monitored gene expression levels of *IRF7* and *IFIT1* in these cells by qPCR. For this assay, we developed and utilized recombinant human IFNβ1. To demonstrate the antiviral efficacy of our recombinant IFN, we pre-treated human fibroblast (THF) cells with IFNβ1, followed by RNA and DNA virus infections. Pre-treatment of THF cells with IFNβ1 inhibited the replication of herpes simplex virus (HSV), vesicular stomatitis virus (VSV) and H1N1 in a dose-dependent manner (*SI Appendix*, Fig. S7).

Exogenous IFNβ treatment alone significantly upregulated transcript levels of *IRF7* and *IFIT1* relative to mock treated Calu-3 cells (Figs. 2H and 2I). Consistent with our RNA-seq data, SARS-CoV-2 infection alone induced significant levels of *IRF7* and *IFIT1* transcripts (Figs. 2H and 2I). However, SARS-CoV-2 induced *IRF7* and *IFIT1* transcript levels were significantly lower compared to levels in both IFNβ treated cells and SARS-CoV-2 infected + IFNβ treated cells (Figs. 2H and 2I). Transcript levels of *IRF7* and *IFIT1* in IFNβ treated cells and SARS-CoV-2 infected + IFNβ treated cells were not significantly different (Figs. 2H and 2I).

Finally, we repeated the experiments with exogenous IFNβ treatment and performed immunoblots to determine if SARS-CoV-2 can modulate type I IFN-mediated upregulation of IFIT1. Exogenous IFNβ treatment alone induced a robust expression of IFIT1 (Fig. 2J). SARS-CoV-2 infection alone was not sufficient for a visible increase in IFIT1 expression in our immunoblots (Fig. 2J). Interestingly, IFNβ treatment after 12 hours of high dose infection (MOI = 2) of SARS-CoV-2 also induced a robust expression of IFIT1 (Fig. 2J). We confirmed SARS-CoV-2 infection in these cells by detecting N protein (Fig. 2J).

Discussion

SARS-CoV-2 emerged in December 2019 and has since caused a global pandemic of COVID-19 (1, 18). Clinical observations and emerging data from *in vitro* and *in vivo* studies have demonstrated the limited ability of SARS-CoV-2 to induce type I IFNs (11). However, the ability of SARS-CoV-2 to modulate IFN production and signaling remains unknown. Furthermore, gene expression kinetics of SARS-CoV-2, along with time-associated host responses have not been described. In this study, we have identified early virus-host interactions using a time-series RNA-seq experiment. Consistent with other studies (11), we demonstrate that a high dose of SARS-CoV-2 induces a type I IFN response; however, our data show that SARS-CoV-2 is

unable to modulate cellular type I IFN production and signaling that are mounted in response to exogenous stimuli.

RNA-seq analysis of poly(A)-enriched RNA allowed us to map the progression of SARS-CoV-2 replication and transcription in Calu-3 cells. As observed with other coronaviruses (19-21), SARS-CoV-2 replicated and transcribed sub-genomic RNA and mRNA in a directional manner (Figs. 1A and 1B). SARS-CoV-2 *N* gene was highly expressed as early as 0 hpi. High MOI of SARS-CoV-2 produced cytopathic effects (CPE) in Calu-3 cells at later time points, which made it difficult to reliably assess host gene expression relative to unstable levels of house-keeping genes.

Coronaviruses, including highly pathogenic SARS-CoV, MERS-CoV and porcine epidemic diarrhea virus (PEDV) have evolved proteins that can efficiently modulate type I IFN responses (7-10, 16, 17, 22, 23). The recently demonstrated inability of SARS-CoV-2 to stimulate the expression of robust amounts of type I IFNs (11) may be associated with its ability to mask the detection of viral RNA by cellular PRRs and/or its ability to inactivate cellular mechanisms involved in type I IFN upregulation. Data from our studies show that SARS-CoV-2 is indeed unable to stimulate high levels of *IFNβ* transcripts relative to poly(I:C) (Fig. 2D). However, SARS-CoV-2 is unable to efficiently shutdown poly(I:C)-mediated upregulation of *IFNβ* transcripts and downstream ISGs (Figs. 2D-F). In fact, poly(I:C) + SARS-CoV-2 induced higher levels of ISG transcripts relative to poly(I:C) alone. Thus, our data hint at additional mechanisms that SARS-CoV-2 may have evolved to mitigate the recognition of viral PAMPs by cellular PRRs. MERS-CoV protein 4a interferes with RIGI and MDA5-mediated sensing of viral RNA (7). Murine hepatitis virus (MHV) encodes an endoribonuclease that cleaves poly-uridine residues in the viral genome, thus limiting the activation of cellular PRRs (24). Endoribonuclease

deficient mouse CoVs induce a robust type I IFN response and can only replicate in cells that are IFN deficient (25, 26). It is possible that SARS-CoV-2 uses a similar strategy to limit the detection of its nucleic acid by cellular PRRs, thus leading to a dampened antiviral IFN response in these cells. Future studies will identify the full breadth of strategies deployed by SARS-CoV-2 to modulate innate antiviral responses.

A recent study has identified the ability of SARS-CoV-2 to replicate to higher titers in the upper respiratory tract, including nasal cells (27). Hou *et al.* have shown that high levels of virus replication in nasal cells is associated with high levels of angiotensin-converting enzyme 2 (ACE2) receptor expression in these cells, relative to cells in the lower respiratory tract (27). Studies have also shown that rhinovirus (common cold virus) replicates to higher titers in nasal cells due to diminished temperature-dependent innate antiviral responses in these cells (28). Thus, the inability of SARS-CoV-2 to induce a robust type I IFN response, coupled with the dampened ability of nasal cells to potentiate an innate immune response may lead to high levels of virus replication in the upper respiratory tract, as observed in COVID-19 patients (29).

In conclusion, our study demonstrates that SARS-CoV-2 is a weak stimulator of type I IFN responses in infected human cells, relative to the more potent form of PAMP, poly(I:C). However, our data suggest that the lack of a robust type I IFN response in SARS-CoV-2 infected cells is likely due to the inability of the cells to recognize viral PAMPs, such as double-stranded RNA. The inability of SARS-CoV-2 to modulate downstream IFN responses is promising for the development of IFNβ as a treatment or post-exposure prophylactic. Clinical trials for combination IFNβ therapy against MERS-CoV are currently ongoing (30). IFNβ, in combination with lopinavir-ritonavir and ribavirin has been used with promising results in COVID-19 patients (31). While it is possible that over-expressing viral proteins may identify interactions that can

modulate type I IFN production in human cells, we did not observe these effects when cells were infected with a high MOI of SARS-CoV-2 and stimulated exogenously. Future studies will shed more light on the full breadth of immune modulatory capabilities of SARS-CoV-2.

Materials and Methods

Cells and viruses. Vero E6 cells (African green monkey cells; ATCC, Manassas, VA, USA) were maintained in Dulbecco's modified Eagle's media (DMEM) supplemented with 10% fetal bovine serum (FBS; Sigma-Aldrich), 1x L-Glutamine and Penicillin/Streptomycin (Pen/Strep; Corning, VWR, Mississauga, ON, Canada). Calu-3 cells (human lung adenocarcinoma derived; ATCC) were cultured as previously mentioned (32). THF cells (human telomerase life-extended cells; from Dr. Victor DeFilippis' lab) were cultured as previously mentioned (33). *Drosophila* S2 cells (ThermoFisher Scientific, Waltham, MA, USA) were cultured in Schneider's *Drosophila* medium supplemented with 10% FBS (Sigma-Aldrich) as recommended by the manufacturer and cells were incubated at 28°C. Stocks of genetically engineered vesicular stomatitis virus (VSV-GFP) carrying a green fluorescent protein (GFP) cassette (34) were stored at -80°C. H1N1 (A/Puerto Rico/8/1934 mNeon – 2A-HA) stocks were obtained from Dr. Matthew Miller's laboratory. HSV-GFP stocks were generated and maintained as mentioned previously (35). SARS-CoV-2/SB3 virus stocks were propagated on Vero E6 cells and validated by next generation sequencing (36). Virus stocks were thawed once and used for an experiment. A fresh vial was used for each experiment to avoid repeated freeze-thaws. VSV-GFP, HSV-GFP and H1N1 infections were performed at an MOI of 1. SARS-CoV-2 infections were performed at an MOI of 2. Experiments with SARS-CoV-2 were performed in a BSL3 laboratory and all procedures were approved by institutional biosafety committees at McMaster University and the University of Toronto.

RNA-Seq

RNA was isolated from cells using RNeasy Mini kit (Qiagen, Hilden, Germany). Sequencing was conducted at the McMaster Genomics Facility, Farncombe Institute at McMaster University. Sample quality was first assessed using a Bioanalyzer (Agilent 2100 Bioanalyzer G2938C, Aligent RNA 6000 Nano Kit, Agilent; Santa Clara, CA, USA), then enriched (NEBNext Poly(A) mRNA Magnetic Isolation Module; NEB, Ipswich, MA, USA). Library preparations were conducted (NEBNext Ultra II Directional RNA Library Prep Kit; NEB, Ipswich, MA, USA) and library fragment size distribution was verified (Agilent TapeSection D1000; Agilent, Santa Clara, CA, USA). Libraries were quantified by qPCR, pooled in equimolar amounts, and qPCR and fragment size distribution verification was conducted again. Libraries were then sequenced on an Illumina HiSeq 1500 across 3 HiSeq Rapid v2 flow cells in 6 lanes (Illumina; San Diego, CA, USA) using a paired-end, 2x50 bp configuration, with onboard cluster generation averaging 30.8M clusters per replicate (minimum 21.9M, maximum 46.0M).

Transcript quantification and differential expression analysis

Sequence read quality was checked with FastQC (https://www.bioinformatics.babraham.ac.uk/projects/fastqc/), with reads subsequently aligned to the human reference transcriptome (GRCh37.67) obtained from the ENSEMBL database (37) , indexed using the 'index' function of Salmon (version 0.14.0) (38) with a k-mer size of 31. Alignment was performed using the Salmon 'quant' function with the following parameters: "-l A --numBootstraps 100 --gcBias --validateMappings". All other parameters were left to defaults. Salmon quantification files were imported into R (version 3.6.1) (39) using the tximport library (version 1.14.0) (40) with the 'type' option set to 'salmon'. Transcript counts were summarized at the gene-level using the corresponding transcriptome GTF file mappings obtained from

ENSEMBL. Count data was subsequently loaded into DESeq2 (version 1.26.0) (41) using the 'DESeqDataSetFromTximport' function. In order to determine time/treatment dependent expression of genes, count data was normalized using the 'estimateSizeFactors' function using the default 'median ratio method' and output using the 'counts' function with the 'normalized' option.

For subsequent differential-expression analysis, a low-count filter was applied prior to normalization, wherein a gene must have had a count greater than 5 in at least three samples in order to be retained. Using all samples, this resulted in the removal of 12,980 genes for a final set of 15,760 used. Principal Component Analysis (PCA) of samples across genes was performed using the 'vst' function in DESeq2 (default settings) and was subsequently plotted with the ggplot2 package in R (42). Differential expression analyses were carried out with three designs: (a) the difference between infection/control status across all timepoints, (b) considering the effects of post-infection time (i.e. the interaction term between time and infection status) and (c) the difference between infection/control status at individual timepoints. (a) and (b) were performed using the 'DESeq' function of DESeq2 using all samples, with results subsequently summarized using the 'results' function with the 'alpha' parameter set to 0.05; *p*-values were adjusted using the Benjamini-Hochberg FDR method (43), with differentially expressed genes filtered for those falling below an adjusted *p*-value of 0.05. For (c), infected/mock samples were subset to individual timepoints, with differential expression calculated using DESeq as described above. Additionally, given the smaller number of samples at individual time-points, differential-expression analysis was also performed with relaxation of the low-count filter described above, with results and p-value adjustments performed as above.

Viral transcript quantification

Paired-end sequencing reads were mapped to CDS regions of the SARS-CoV-2 genomic sequence (Assembly ASM985889v3 - GCF_009858895.2) obtained from NCBI, indexed using the 'index' function of Salmon (version 0.14.0) (38) with a k-mer size of 31. Subsequently, reads were aligned using the Salmon 'quant' function with the following parameters: "-l A --numBootstraps 100 --gcBias --validateMappings". All other parameters were left to defaults. Salmon quantification files were imported into R (version 3.6.1) (39) using the tximport library (version 1.14.0) (40) with the 'type' option set to 'salmon'. All other parameters were set to default. Transcripts were mapped to their corresponding gene products via GTF files obtained from NCBI. Count data was subsequently loaded into DESeq2 (version 1.26.0) (41) using the 'DESeqDataSetFromTximport' function. Principal Component Analysis (PCA) of samples across viral genes was performed using the 'vst' function in DESeq2 (default settings) and was subsequently plotted with the ggplot2 package in R (42). As viral transcript levels increased over time post-infection, we first converted non-normalized transcript counts to a $\log_2$ scale, and subsequently compared these across time-points (Fig. 1B; *SI Appendix*, Table S1). To look at the changes in the expression of viral transcripts relative to total viral expression as a function of post-infection time, normalized transcript counts were used to perform differential-expression analysis with DESeq2. Results and p-value adjustments were performed as described above.

In order to compare host/viral expression patterns, normalized transcript counts from infected samples were compared with either normalized or non-normalized viral transcript counts (from the same sample) across time-points. For each viral transcript (n = 12), all host genes (n = 15,760, after filtering described above) were tested for correlated expression changes across matched infected samples (n = 18, across 5 time-points) using Pearson's correlation coefficient (via the cor.test function in R). Correlation test *p*-values were adjusted across all-by-

all comparisons using the Benjamini-Hochberg FDR method, and gene-transcript pairs at adjusted *p*-value < 0.05 were retained. To account for possible effects of cellular response to plate incubation, viral transcript abundance was averaged at each time-point and compared to host transcript abundance similarly averaged at each time-point for non-infected samples; correlation testing was done all-by-all for n = 5 data-points. Host genes that correlated with viral transcription in mock samples across time were removed from subsequent analyses; to increase stringency, mock correlation was defined using un-adjusted *p*-value < 0.05. Host genes were sorted by correlation coefficient (with any given viral transcript), with the top 100 unique genes retained for visualization. Normalized host transcript counts were z-score transformed per-gene using the 'scale' function in R, with normalized/un-normalized viral transcript counts similarly transformed per-transcript. Resulting z-score expression heatmaps were generated using the ComplexHeatmap library in R (version 2.2.0) (44). Heatmaps were generated for normalized/un-normalized viral transcript counts, given the different information revealed by absolute and relative viral expression patterns.

Viral genome mapping

Paired-end RNA-seq reads were filtered for quality control with Trim Galore! (version 0.6.4_dev) (45) and mapped to the SARS-CoV-2 reference sequence (NC_045512.2) with the Burrow-Wheeler Aligner (46), using the BWA-MEM algorithm (47). Output SAM files were sorted and compressed into BAM files using Samtools (version 1.10) (48). Read coverage visualization was performed from within the R statistical environment (version 4.0.0) (39) using the "scanBam" function from the Rsamtools R package (version 1.32.0) to extract read coverage data and the ggplot2 R package (version 3.3.0) (42) to plot read coverage histograms (using 300 bins across the SARS-CoV-2 sequence).

Cellular pathway enrichment analysis

To determine cellular pathways that were associated with differentially expressed genes (DEGs), the ActivePathways R (version 1.0.1) (49) package was utilized to perform gene-set based pathway enrichment analysis. DEGs at each time point were treated as an independent set for enrichment analysis. Fisher's combined probability test was used to enrich pathways after *p*-value adjustment using Holm-Bonferroni correction. Pathways of gene-set size less than 5 and greater than 1000 were excluded. Only pathways enriched at individual time-points were considered for downstream analysis; pathways enriched across combined timepoints as determined by ActivePathways Brown's *p*-value merging method were filtered out. Visualization of enriched pathways across timepoints was done using Cytoscape (version 3.8.0) (50) and the EnrichmentMap plugin (version 3.2.1) (51), as outlined by Reimand *et al*. (52). Up-to-date Gene-Matrix-Transposed (GMT) files containing information on pathways for the Gene Ontology (GO) Molecular Function (MF), GO Biological Process (BP) (53) and REACTOME (54) pathway databases were utilized with ActivePathways. Only pathways that were enriched at specific time points were considered. Bar plots displaying top ActivePathway GO terms and REACTOME enrichments for infection versus mock were plotted using the ggplot2 R package (version 3.2.1) for 1, 2, 3, and 12 hour time points. Zero and 6 hour time points were omitted due to a lack of sufficient numbers of differentially expressed genes required for functional enrichment analysis.

Poly(I:C) transfection and IFNβ treatment. Calu-3 cells were mock transfected with 4 µl of lipofectamine 3000 (ThermoFisher Scientific) only or transfected with 100 ng of poly(I:C) (InvivoGen, San Diego, CA, USA). Recombinant human IFNβ1 was generated using *Drosophila* Schneider 2 (S2) cells following manufacturer's recommendation and by using ThermoFisher

Scientific's *Drosophila* Expression system. As a control, recombinant GFP was also generated using the same protocol and used for mock treated cells. For VSV-GFP, HSV-GFP and H1N1-mNeon infections, cells were treated with increasing concentrations of IFNβ1 or GFP (control). SARS-CoV-2 infected cells were treated with 200 μg/ml of IFNβ1 or GFP.

Quantitative PCR. Calu-3 cells were seeded at a density of 3 x 10^5 cells/well in 12-well plates. Cells were infected with SARS-CoV-2 and RNA extraction was performed using RNeasy® Mini Kit (Qiagen, Hilden, Germany) according to manufacturer's protocol. 200 ng of purified RNA was reverse transcribed using iScript™ gDNA Clear cDNA Synthesis Kit (Bio-Rad, Hercules, CA, USA). Quantitative PCR reactions were performed with TaqMan™ Universal PCR Master Mix (Applied Biosystems, Foster City, CA, USA) using pre-designed Taqman gene expression assays (ThermoFisher Scientific) for *IFNβ1* (catalog #4331182), *IRF7* (catalog #4331182), *IFIT1* (catalog #4331182) and *GAPDH* (catalog #4331182) according to manufacturer's protocol. Relative mRNA expression was normalized to *GAPDH* and presented as 1/ΔCt.

Immunoblots. Calu-3 cells were seeded at a density of 3 x 10^5 cells/well in 12-well plates. Cells were infected with SARS-CoV-2 at an MOI of 2. Control cells were sham infected. Twelve hours post infection, cells were transfected or treated with poly(I:C) or IFNβ, respectively. Cell lysates were harvested for immunoblots and analyzed on reducing gels as mentioned previously (33). Briefly, samples were denatured in a reducing sample buffer and analyzed on a reducing gel. Proteins were blotted from the gel onto polyvinylidene difluoride (PVDF) membranes (Immobilon, EMD Millipore, Burlington, MA, USA) and detected using primary and secondary antibodies. Primary antibodies used were: 1:1000 mouse anti-GAPDH (EMD Millipore; Catalogue number: AB2302; RRID: AB_10615768), 1:1000 mouse anti-SARS-CoV-2 N (ThermoFisher Scientific; Catalogue number: MA5-29981; RRID: AB_2785780 and 1:1000

rabbit anti-IFIT1 (ThermoFisher Scientific; Catalogue number: PA3-848; RRID: AB_1958733). Secondary antibodies used were: 1:5000 donkey anti-rabbit 800 (LI-COR Biosciences, Lincoln, NE, USA; Catalogue number: 926-32213; RRID: 621848) and 1:5000 goat anti-mouse 680 (LI-COR Biosciences; Catalogue number: 925-68070; RRID: AB_2651128). Blots were observed and imaged using Image Studio (LI-COR Biosciences) on the Odyssey CLx imaging system (LI-COR Biosciences).

Antiviral bioassay. THF cells were pre-treated or mock treated with recombinant human IFNβ, followed by VSV-GFP, HSV-GFP or H1N1-mNeon infection at an MOI of 1. Infected cells were incubated at 37°C for 1 hour with gentle rocking every 15 minutes. After 1 hr, virus inoculum was aspirated and Minimum Essential Medium (MEM) with Earle's salts (Sigma) containing 2% FBS and 1% carboxymethyl cellulose (CMC; Sigma) was added on the cells. Cells were incubated for 19 hours at 37°C and green fluorescent protein (GFP) or mNeon levels were measured using a typhoon scanner (Amersham, GE Healthcare, Chicago, IL, USA).

Statistics. Statistical analyses for RNA-seq data were performed in R and are mentioned under the respective RNA-seq analyses sections. All other statistical calculations were performed in GraphPad Prism (version 8.4.2; www.graphpad.com) using two-tailed paired t-test. Significance values are indicated in the figures and figure legends. p*<0.05, **<0.01, ***<0.001 and ****<0.0001.

Data Availability

The DESeq2 normalized transcript counts for all genes with RNA-Seq data, significant or otherwise, plus the raw sequencing FASTQ reads have been deposited into the Gene Expression Omnibus (GEO) database with NCBI GEO accession number GSE151513.

Acknowledgements

This study was supported by a Canadian Institutes of Health Research (CIHR) COVID-19 rapid response grant to principal applicant K.M. and Co-Applicants A.B., A.G.M., M.S.M. and S.M. A.B. was funded by the Natural Sciences and Engineering Research Council of Canada (NSERC). Computer resources were in part supplied by the McMaster Service Lab and Repository computing cluster, funded in part by grants to A.G.M. from the Canadian Foundation for Innovation. J.A.H. is supported by the Canada Research Chairs Program and an Ontario Early Career Researcher Award. M.S.M. is supported by a CIHR COVID-19 rapid response grant, a CIHR New Investigator Award and an Ontario Early Researcher Award.

References

1. P. Zhou *et al.*, A pneumonia outbreak associated with a new coronavirus of probable bat origin. *Nature* **579**, 270-273 (2020).
2. T. Kawai, S. Akira, Innate immune recognition of viral infection. *Nat Immunol* **7**, 131-137 (2006).
3. S. Koyama, K. J. Ishii, C. Coban, S. Akira, Innate immune response to viral infection. *Cytokine* **43**, 336-341 (2008).
4. K. S. Schulz, K. L. Mossman, Viral Evasion Strategies in Type I IFN Signaling - A Summary of Recent Developments. *Front Immunol* **7**, 498 (2016).
5. M. G. Katze, Y. He, M. Gale, Jr., Viruses and interferon: a fight for supremacy. *Nat Rev Immunol* **2**, 675-687 (2002).
6. E. de Wit, N. van Doremalen, D. Falzarano, V. J. Munster, SARS and MERS: recent insights into emerging coronaviruses. *Nat Rev Microbiol* **14**, 523-534 (2016).

7. K. L. Siu *et al.*, Middle east respiratory syndrome coronavirus 4a protein is a double-stranded RNA-binding protein that suppresses PACT-induced activation of RIG-I and MDA5 in the innate antiviral response. *J Virol* **88**, 4866-4876 (2014).

8. X. Lu, J. Pan, J. Tao, D. Guo, SARS-CoV nucleocapsid protein antagonizes IFN-beta response by targeting initial step of IFN-beta induction pathway, and its C-terminal region is critical for the antagonism. *Virus Genes* **42**, 37-45 (2011).

9. X. Chen *et al.*, SARS coronavirus papain-like protease inhibits the type I interferon signaling pathway through interaction with the STING-TRAF3-TBK1 complex. *Protein Cell* **5**, 369-381 (2014).

10. Y. Yang *et al.*, The structural and accessory proteins M, ORF 4a, ORF 4b, and ORF 5 of Middle East respiratory syndrome coronavirus (MERS-CoV) are potent interferon antagonists. *Protein Cell* **4**, 951-961 (2013).

11. D. Blanco-Melo *et al.*, Imbalanced Host Response to SARS-CoV-2 Drives Development of COVID-19. *Cell* 10.1016/j.cell.2020.04.026 (2020).

12. J. Hadjadj *et al.*, Impaired type I interferon activity and exacerbated inflammatory responses in severe Covid-19 patients. *medRxiv* 10.1101/2020.04.19.20068015 (2020).

13. S. Trouillet-Assant *et al.*, Type I IFN immunoprofiling in COVID-19 patients. *J Allergy Clin Immunol* 10.1016/j.jaci.2020.04.029 (2020).

14. A. Banerjee, K. Baid, K. Mossman, Molecular Pathogenesis of Middle East Respiratory Syndrome (MERS) Coronavirus. *Curr Clin Microbiol Rep* **6**, 139-147 (2019).

15. S. G. Sawicki, D. L. Sawicki, S. G. Siddell, A contemporary view of coronavirus transcription. *J Virol* **81**, 20-29 (2007).

16. D. Niemeyer *et al.*, Middle East respiratory syndrome coronavirus accessory protein 4a is a type I interferon antagonist. *J Virol* **87**, 12489-12495 (2013).

17. P. Y. Lui *et al.*, Middle East respiratory syndrome coronavirus M protein suppresses type I interferon expression through the inhibition of TBK1-dependent phosphorylation of IRF3. *Emerg Microbes Infect* **5**, e39 (2016).

18. E. Dong, H. Du, L. Gardner, An interactive web-based dashboard to track COVID-19 in real time. *Lancet Infect Dis* **20**, 533-534 (2020).

19. M. M. Lai, Coronavirus: organization, replication and expression of genome. *Annu Rev Microbiol* **44**, 303-333 (1990).

20. S. Perlman, J. Netland, Coronaviruses post-SARS: update on replication and pathogenesis. *Nat Rev Microbiol* **7**, 439-450 (2009).

21. A. R. Fehr, S. Perlman, Coronaviruses: an overview of their replication and pathogenesis. *Methods Mol Biol* **1282**, 1-23 (2015).

22. Y. Xing *et al.*, The papain-like protease of porcine epidemic diarrhea virus negatively regulates type I interferon pathway by acting as a viral deubiquitinase. *J Gen Virol* **94**, 1554-1567 (2013).

23. Z. Ding *et al.*, Porcine epidemic diarrhea virus nucleocapsid protein antagonizes beta interferon production by sequestering the interaction between IRF3 and TBK1. *J Virol* **88**, 8936-8945 (2014).

24. M. Hackbart, X. Deng, S. C. Baker, Coronavirus endoribonuclease targets viral polyuridine sequences to evade activating host sensors. *Proc Natl Acad Sci U S A* **117**, 8094-8103 (2020).

25. X. Deng *et al.*, Coronavirus nonstructural protein 15 mediates evasion of dsRNA sensors and limits apoptosis in macrophages. *Proc Natl Acad Sci U S A* **114**, E4251-E4260 (2017).

26. E. Kindler *et al.*, Early endonuclease-mediated evasion of RNA sensing ensures efficient coronavirus replication. *PLoS Pathog* **13**, e1006195 (2017).

27. Y. J. Hou *et al.*, SARS-CoV-2 Reverse Genetics Reveals a Variable Infection Gradient in the Respiratory Tract. *Cell* 10.1016/j.cell.2020.05.042 (2020).

28. E. F. Foxman *et al.*, Temperature-dependent innate defense against the common cold virus limits viral replication at warm temperature in mouse airway cells. *Proc Natl Acad Sci U S A* **112**, 827-832 (2015).

29. R. Wolfel *et al.*, Virological assessment of hospitalized patients with COVID-2019. *Nature* 10.1038/s41586-020-2196-x (2020).

30. Y. M. Arabi *et al.*, Treatment of Middle East respiratory syndrome with a combination of lopinavir/ritonavir and interferon-beta1b (MIRACLE trial): statistical analysis plan for a recursive two-stage group sequential randomized controlled trial. *Trials* **21**, 8 (2020).

31. I. F.-N. Hung *et al.*, Triple combination of interferon beta-1b, lopinavir–ritonavir, and ribavirin in the treatment of patients admitted to hospital with COVID-19: an open-label, randomised, phase 2 trial. *The Lancet* **395**, 1695-1704 (2020).

32. J. A. Aguiar *et al.*, Transcriptomic and barrier responses of human airway epithelial cells exposed to cannabis smoke. *Physiol Rep* **7**, e14249 (2019).

33. A. Banerjee *et al.*, Positive Selection of a Serine Residue in Bat IRF3 Confers Enhanced Antiviral Protection. *iScience* **23**, 100958 (2020).

34. R. S. Noyce *et al.*, Membrane perturbation elicits an IRF3-dependent, interferon-independent antiviral response. *J Virol* **85**, 10926-10931 (2011).

35. R. L. Minaker, K. L. Mossman, J. R. Smiley, Functional inaccessibility of quiescent herpes simplex virus genomes. *Virol J* **2**, 85 (2005).

36. A. Banerjee *et al.*, Isolation, sequence, infectivity, and replication kinetics of Severe Acute Respiratory Syndrome Coronavirus 2. *Emerging Infectious Diseases* ***In Press*** (2020).

37. S. E. Hunt *et al.*, Ensembl variation resources. *Database (Oxford)* **2018** (2018).

38. R. Patro, G. Duggal, M. I. Love, R. A. Irizarry, C. Kingsford, Salmon provides fast and bias-aware quantification of transcript expression. *Nat Methods* **14**, 417-419 (2017).

39. RCoreTeam (2017) R: A language and environment for statistical computing.

40. C. Soneson, M. I. Love, M. D. Robinson, Differential analyses for RNA-seq: transcript-level estimates improve gene-level inferences. *F1000Research* **4** (2015).

41. M. I. Love, W. Huber, S. Anders, Moderated estimation of fold change and dispersion for RNA-seq data with DESeq2. *Genome Biol* **15**, 550 (2014).

42. H. Wickham, *ggplot2: Elegant graphics for data analysis* (Springer-Verlag, New York, 2009).

43. Y. Benjamini, Y. Hochberg, Controlling the False Discovery Rate: A Practical and Powerful Approach to Multiple Testing. *Journal of the Royal Statistical Society: Series B (Methodological)* **57**, 289-300 (1995).

44. Z. Gu, R. Eils, M. Schlesner, Complex heatmaps reveal patterns and correlations in multidimensional genomic data. *Bioinformatics* **32**, 2847-2849 (2016).

45. F. Krueger (2019) Trim Galore.

46. H. Li, R. Durbin, Fast and accurate short read alignment with Burrows-Wheeler transform. *Bioinformatics* **25**, 1754-1760 (2009).

47. H. Li, Aligning sequence reads, clone sequences and assembly contigs with BWA-MEM. *arXiv:1303.3997 [q-bio.GN]* (2013).

48. H. Li *et al.*, The Sequence Alignment/Map format and SAMtools. *Bioinformatics* **25**, 2078-2079 (2009).

49. M. Paczkowska *et al.*, Integrative pathway enrichment analysis of multivariate omics data. *Nat Commun* **11**, 735 (2020).

50. P. Shannon *et al.*, Cytoscape: a software environment for integrated models of biomolecular interaction networks. *Genome Res* **13**, 2498-2504 (2003).

51. D. Merico, R. Isserlin, O. Stueker, A. Emili, G. D. Bader, Enrichment map: a network-based method for gene-set enrichment visualization and interpretation. *PLoS One* **5**, e13984 (2010).

52. J. Reimand *et al.*, Pathway enrichment analysis and visualization of omics data using g:Profiler, GSEA, Cytoscape and EnrichmentMap. *Nat Protoc* **14**, 482-517 (2019).

53. C. The Gene Ontology, The Gene Ontology Resource: 20 years and still GOing strong. *Nucleic Acids Res* **47**, D330-D338 (2019).

54. B. Jassal *et al.*, The reactome pathway knowledgebase. *Nucleic Acids Res* **48**, D498-D503 (2020).

Figures and Figure Legends

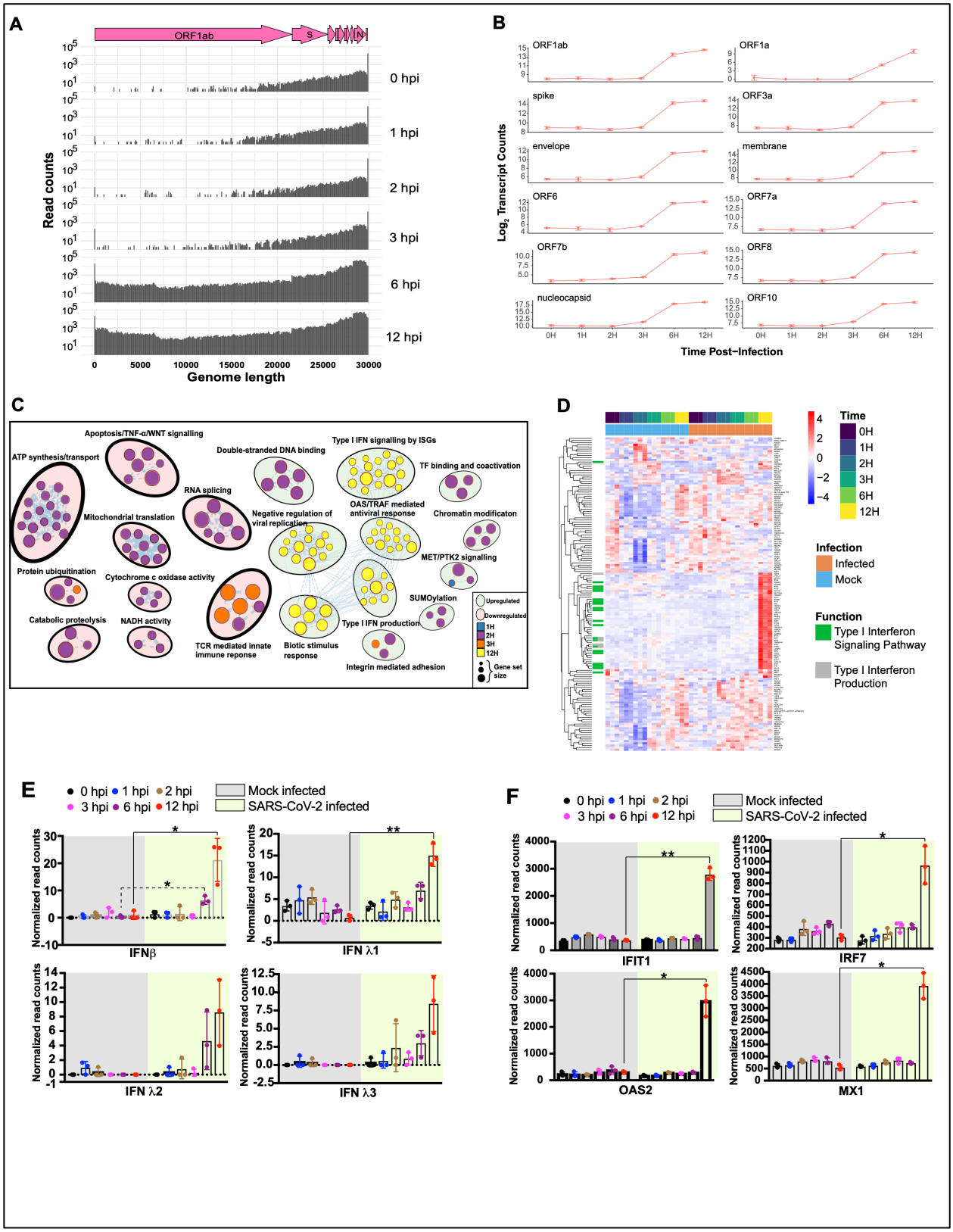

595 **Figure 1. SARS-CoV-2 and cellular gene expression.** Calu-3 cells were infected with SARS-
596 CoV-2 at an MOI of 2. Virus and host gene expression were determined using time-series RNA-
597 seq analyses. **(A)** SARS-CoV-2 gene expression over 12 hours (n = 3/time point). The genome
598 organization of SARS-CoV-2 is indicated above in pink. **(B)** Major SARS-CoV-2 gene
599 expression levels at different times post infection (n = 3/time point). **(C)** Cellular processes that
600 are down or upregulated at different times post infection. The size of the circles represents the
601 number of genes that are down or upregulated at different times after infection (n = 3/time point).
602 **(D)** Cellular genes (n = 124) that are significantly up or downregulated (FDR-adjusted $p<0.05$;
603 $|\log_2 FC| > 1$) in SARS-CoV-2 infected cells, relative to mock infected cells at different times
604 post infection. Transcript levels are shown as z-score normalized expression (scaled by gene).
605 **(E)** Transcript abundance of type I interferon (IFN) genes (*IFNβ* and *IFNλ1-3*) in mock infected
606 and SARS-CoV-2 infected Calu-3 cells at different times (Mean ± SD; n = 3). **(F)** Transcript
607 abundance of representative interferon stimulated genes (ISGs) in mock infected and SARS-
608 CoV-2 infected Calu-3 cells at different times (Mean ± SD; n = 3). For Figs. A-D, statistical
609 analysis was performed in R (see methods). For Figs. E and F, statistical significance was
610 calculated using two-tailed paired t-test. hpi, hours post infection. p*<0.05, **<0.01.
611

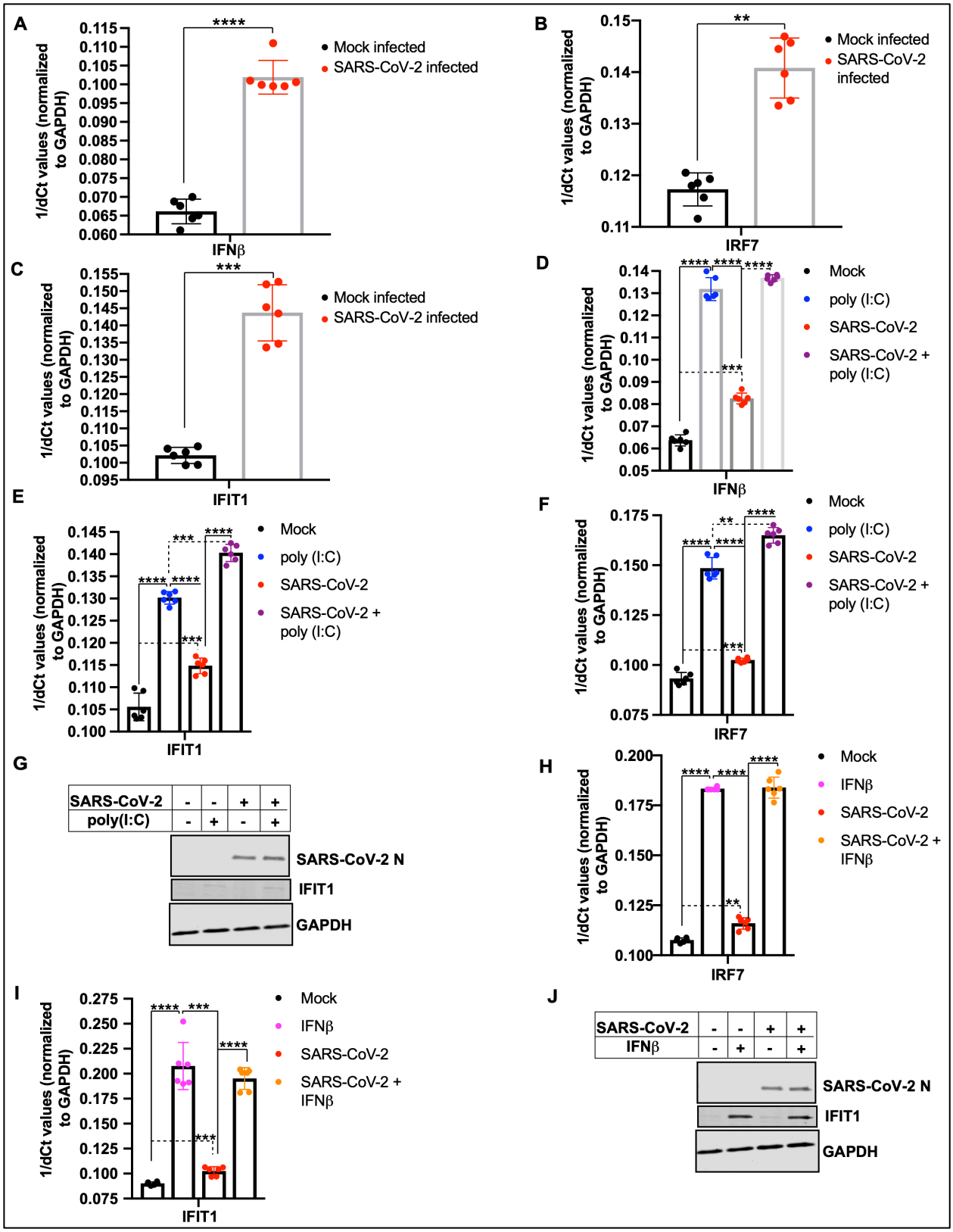

612

Figure 2. SARS-CoV-2 is unable to modulate type I IFN gene expression and downstream ISG production. To determine if SARS-CoV-2 is able to induce type I IFN production, Calu-3 cells were infected at an MOI of 2 for 12 hours. Transcript levels for *IFNβ* were quantified using qPCR. To assess if SARS-CoV-2 can modulate *IFNβ* gene expression and downstream stimulation of ISGs, Calu-3 cells were infected with SARS-CoV-2 at an MOI of 2 for 12 hours, following which cells were treated or transfected with recombinant IFNβ or poly(I:C), respectively for 6 hours. Mock infected and mock treated cells served as controls. **(A)** *IFNβ* transcript levels in SARS-CoV-2 infected or mock infected Calu-3 cells, normalized to *GAPDH* (Mean ± SD; n = 6). **(B)** *IRF7* transcript levels in SARS-CoV-2 infected or mock infected Calu-3 cells, normalized to *GAPDH* (Mean ± SD; n = 6). **(C)** *IFIT1* transcript levels in SARS-CoV-2 infected or mock infected Calu-3 cells, normalized to *GAPDH* (Mean ± SD; n = 6). **(D)** *IFNβ* transcript levels in SARS-CoV-2 infected or mock infected, and poly(I:C) transfected or mock transfected Calu-3 cells, normalized to *GAPDH* (Mean ± SD; n = 6). **(E)** *IFIT1* transcript levels in SARS-CoV-2 infected or mock infected, and poly(I:C) transfected or mock transfected Calu-3 cells, normalized to *GAPDH* (Mean ± SD; n = 6). **(F)** *IRF7* transcript levels in SARS-CoV-2 infected or mock infected, and poly(I:C) transfected or mock transfected Calu-3 cells, normalized to *GAPDH* (Mean ± SD; n = 6). **(G)** SARS-CoV-2 N, IFIT1 and GAPDH protein expression in SARS-CoV-2 infected or mock infected, and poly(I:C) transfected or mock transfected Calu-3 cells (Mean ± SD; n = 3). **(H)** *IRF7* transcript levels in SARS-CoV-2 infected or mock infected, and recombinant IFNβ treated or mock treated Calu-3 cells, normalized to *GAPDH* (Mean ± SD; n = 6). **(I)** *IFIT1* transcript levels in SARS-CoV-2 infected or mock infected, and recombinant IFNβ treated or mock treated Calu-3 cells, normalized to *GAPDH* (Mean ± SD; n = 6). (J) SARS-CoV-2 N, IFIT1 and GAPDH protein expression in SARS-CoV-2

infected or mock infected, and recombinant IFNβ treated or mock treated Calu-3 cells (Mean ± SD; n = 3). Statistical significance was calculated using two-tailed paired t-test. Ct, cycle threshold. *p**<0.05, **<0.01, ***<0.001 and ****<0.0001.

SI Appendix

Tables

Table S1. Mean raw read counts for SARS-CoV-2 genes. INF, SARS-CoV-2 infected; H, hours; SD, standard deviation.

Mean INF 0H	SD INF 0H	Mean INF 1H	SD INF 1H	Mean INF 2H	SD INF 2H	Mean INF 3H	SD INF 3H	Mean INF 6H	SD INF 6H	Mean INF 12H	SD INF 12H	SARS-CoV-2 gene	Transcript
257.67	38.59	285.33	56.13	243.67	39.25	278.00	23.00	12173.33	3006.93	25827.33	2054.93	ORF1ab	lcl|NC_045512.2_cds_YP_009724389.1_1
1.00	1.73	0.00	0.00	0.33	0.58	0.00	0.00	33.67	6.81	1061.00	468.03	ORF1a	lcl|NC_045512.2_cds_YP_009725295.1_2
500.67	94.52	491.33	86.19	378.00	61.39	521.67	49.69	19232.33	3952.46	26903.33	3860.82	spike	lcl|NC_045512.2_cds_YP_009724390.1_3
173.67	24.99	172.33	43.68	127.33	17.16	203.33	26.50	9995.00	1736.00	13976.33	2233.55	ORF3a	lcl|NC_045512.2_cds_YP_009724391.1_4
43.67	5.51	44.67	13.65	39.00	2.65	63.00	11.53	2903.33	485.15	4086.33	627.70	envelope	lcl|NC_045512.2_cds_YP_009724392.1_5
199.67	27.02	196.00	37.32	162.33	28.87	298.67	19.60	22344.33	3354.18	31200.33	4915.23	membrane	lcl|NC_045512.2_cds_YP_009724393.1_6
34.67	2.08	32.33	10.50	25.00	7.81	45.33	1.53	3508.00	509.12	4704.67	886.56	ORF6	lcl|NC_045512.2_cds_YP_009724394.1_7
107.33	19.50	102.33	23.35	94.00	22.61	173.67	34.00	14834.00	2357.53	21920.67	3441.71	ORF7a	lcl|NC_045512.2_cds_YP_009724395.1_8
10.33	2.52	11.67	2.31	15.33	1.53	20.67	1.15	1516.33	241.00	2191.33	526.17	ORF7b	lcl|NC_045512.2_cds_YP_009725318.1_9
109.33	22.19	107.00	27.22	98.00	21.70	189.00	14.00	14651.33	2136.80	21518.67	3992.04	ORF8	lcl|NC_045512.2_cds_YP_009724396.1_10
1251.00	230.97	1157.33	247.52	1067.67	144.58	2945.67	402.61	258553.00	34843.96	393221.67	62159.07	nucleocapsid	lcl|NC_045512.2_cds_YP_009724397.2_11
112.33	27.57	97.00	22.52	94.67	10.69	250.00	19.00	18385.33	2239.71	27679.00	5406.01	ORF10	lcl|NC_045512.2_cds_YP_009725255.1_12

Table S2. Mean normalized read counts for differentially expressed IFN and ISG transcripts. H, hour; INF, SARS-CoV-2 infected; MOCK, mock infected; IFN, interferon; ISG, interferon stimulated genes.

		0H INF (N=3)	0H MOCK (N=3)	1H INF (N=3)	1H MOCK (N=3)	2H INF (N=3)	2H MOCK (N=3)	3H INF (N=3)	3H MOCK (N=3)	6H INF (N=3)	6H MOCK (N=3)	12H INF (N=3)	12H MOCK (N=3)
IFNs	IFNB1	1.35	0.00	1.21	0.41	1.48	0.97	0.57	1.93	6.40	0.30	21.23	0.89
	IFNL1	3.49	3.45	2.20	4.80	4.93	5.46	3.17	1.90	7.00	2.66	15.07	0.73
	IFNL2	0.00	0.00	0.36	0.96	4.11	0.35	0.28	0.00	4.66	0.00	8.61	0.00
	IFNL3	0.35	0.00	0.58	0.44	2.38	0.31	0.88	0.00	3.02	0.00	8.46	0.00
ISGs	IFIT1	388.42	358.77	370.80	487.33	447.59	590.32	425.31	498.05	463.17	408.65	2790.57	367.50
	IRF7	278.50	283.73	320.43	284.00	339.99	383.89	399.07	363.67	399.93	432.29	966.54	305.31
	OAS2	172.67	236.24	178.18	222.85	287.61	208.20	252.85	296.10	292.36	378.90	2979.22	303.60
	MX1	588.48	620.75	624.79	647.52	758.95	800.13	839.47	867.29	728.29	811.68	3922.41	546.94
	RSAD2	204.76	216.53	228.73	272.67	313.84	348.31	365.12	393.68	274.53	269.56	948.75	210.54
	SLC44A4	1247.82	1171.72	1218.77	1046.17	1138.09	1128.19	1129.60	1106.06	1010.30	1142.19	1032.09	1298.09
	IFIH1	1052.81	1100.39	1134.78	1163.76	1235.36	1164.31	1223.66	1371.55	1189.70	1191.00	2492.69	1087.88
	GBP1	506.79	512.73	503.57	608.29	496.74	485.28	458.14	509.15	530.04	509.53	1151.35	488.92
	IFI44	689.16	741.40	789.19	803.61	963.68	1113.99	997.06	1052.67	785.42	782.39	1889.54	671.51
	IFI27	311.49	318.74	302.63	399.59	343.37	472.30	328.28	361.48	333.63	351.85	921.55	342.54
	IFI6	592.82	612.04	599.90	697.80	673.06	1010.20	692.26	752.25	729.19	775.17	2066.30	709.85
	ISG15	430.95	447.57	443.60	533.02	465.88	704.43	490.49	554.07	473.88	502.97	1260.48	435.91
	IFIT2	657.23	698.02	676.46	795.49	645.57	732.08	455.75	504.29	493.48	422.04	1465.16	413.27
	USP18	212.27	217.53	218.01	257.03	253.55	301.50	266.17	297.44	243.57	232.66	873.18	218.27
	IFIT3	648.15	656.89	747.61	858.17	810.13	1069.67	567.26	668.13	458.25	428.90	1900.07	420.64
	CMPK2	163.89	179.41	169.11	182.05	219.35	244.03	235.97	265.54	172.78	201.60	906.22	153.23
	XAF1	58.53	82.76	73.40	53.61	69.79	60.14	79.67	55.09	86.30	91.97	513.01	90.51
	IFITM1	27.68	34.25	21.94	27.89	28.53	53.49	26.88	34.91	34.59	35.75	182.01	34.33
	MX2	82.11	87.24	69.22	81.96	100.75	83.43	87.84	87.48	108.05	78.88	547.98	64.92

683 **Table S3.** Pathway enrichment analysis. Significance was determined after FDR correction. H,
684 hour; 0, non-significant; 1, significant.
685

term.id	term.name	adjusted.p.val	1H	2H	3H	12H
GO:0000976	transcription regulatory region sequence-specific DNA binding	0.004824255	0	1	0	0
GO:0001067	regulatory region nucleic acid binding	0.004203707	0	1	0	0
GO:0001816	cytokine production	0.005529472	0	0	0	1
GO:0001817	regulation of cytokine production	0.001829233	0	0	0	1
GO:0002230	positive regulation of defense response to virus by host	0.002197834	0	0	0	1
GO:0002831	regulation of response to biotic stimulus	8.60E-08	0	0	0	1
GO:0002833	positive regulation of response to biotic stimulus	0.008687053	0	0	0	1
GO:0003690	double-stranded DNA binding	0.000112873	0	1	0	0
GO:0003712	transcription coregulator activity	1.30E-06	0	1	0	0
GO:0003713	transcription coactivator activity	2.39E-05	0	1	0	0
GO:0005178	integrin binding	0.013874905	0	0	1	0
GO:0008270	zinc ion binding	0.000103938	0	1	0	0
GO:0009615	response to virus	1.39E-35	0	0	0	1
GO:0010810	regulation of cell-substrate adhesion	0.008350323	0	1	0	0
GO:0016482	cytosolic transport	0.011086056	0	1	0	0
GO:0019058	viral life cycle	3.92E-11	0	0	0	1
GO:0019079	viral genome replication	3.87E-15	0	0	0	1
GO:0019221	cytokine-mediated signaling pathway	8.45E-16	0	0	0	1
GO:0019900	kinase binding	0.003539788	0	1	0	0
GO:0019901	protein kinase binding	0.012867428	0	1	0	0
GO:0030099	myeloid cell differentiation	0.011382292	0	1	0	0
GO:0031347	regulation of defense response	2.16E-05	0	0	0	1
GO:0031589	cell-substrate adhesion	0.002867293	0	1	0	0
GO:0032020	ISG15-protein conjugation	0.008627708	0	0	0	1
GO:0032069	regulation of nuclease activity	1.26E-06	0	0	0	1
GO:0032479	regulation of type I interferon production	4.92E-06	0	0	0	1
GO:0032480	negative regulation of type I interferon production	0.005210998	0	0	0	1
GO:0032481	positive regulation of type I interferon production	0.00531473	0	0	0	1
GO:0032606	type I interferon production	6.14E-06	0	0	0	1
GO:0032607	interferon-alpha production	0.005237546	0	0	0	1
GO:0032647	regulation of interferon-alpha production	0.00400414	0	0	0	1
GO:0032727	positive regulation of interferon-alpha production	0.001567461	0	0	0	1
GO:0034340	response to type I interferon	9.21E-31	0	0	0	1
GO:0034341	response to interferon-gamma	1.44E-10	0	0	0	1
GO:0034504	protein localization to nucleus	0.00295333	0	1	0	0
GO:0035455	response to interferon-alpha	3.29E-10	0	0	0	1
GO:0035456	response to interferon-beta	2.08E-07	0	0	0	1

GO:0042393	histone binding	0.002987285	0	1	0	0
GO:0043900	regulation of multi-organism process	2.03E-17	0	0	0	1
GO:0043901	negative regulation of multi-organism process	3.86E-17	0	0	0	1
GO:0043902	positive regulation of multi-organism process	0.008274484	0	0	0	1
GO:0043903	regulation of symbiosis encompassing mutualism through parasitism	6.66E-20	0	0	0	1
GO:0044212	transcription regulatory region DNA binding	0.004047416	0	1	0	0
GO:0045069	regulation of viral genome replication	1.01E-16	0	0	0	1
GO:0045071	negative regulation of viral genome replication	3.61E-17	0	0	0	1
GO:0045088	regulation of innate immune response	5.98E-06	0	0	0	1
GO:0045089	positive regulation of innate immune response	0.005979802	0	0	0	1
GO:0046596	regulation of viral entry into host cell	0.048025337	0	0	0	1
GO:0048525	negative regulation of viral process	3.26E-20	0	0	0	1
GO:0050657	nucleic acid transport	0.048485615	0	0	1	0
GO:0050658	RNA transport	0.048485615	0	0	1	0
GO:0050688	regulation of defense response to virus	0.002163216	0	0	0	1
GO:0050691	regulation of defense response to virus by host	0.009541892	0	0	0	1
GO:0050792	regulation of viral process	1.31E-20	0	0	0	1
GO:0051056	regulation of small GTPase mediated signal transduction	0.026048495	0	1	0	0
GO:0051607	defense response to virus	1.25E-37	0	0	0	1
GO:0060333	interferon-gamma-mediated signaling pathway	1.36E-13	0	0	0	1
GO:0060337	type I interferon signaling pathway	3.69E-31	0	0	0	1
GO:0060700	regulation of ribonuclease activity	6.89E-07	0	0	0	1
GO:0060759	regulation of response to cytokine stimulus	0.000740173	0	0	0	1
GO:0060760	positive regulation of response to cytokine stimulus	0.007105564	0	0	0	1
GO:0061629	RNA polymerase II-specific DNA-binding transcription factor binding	0.011126656	0	1	0	0
GO:0070566	adenylyltransferase activity	0.006545402	0	0	0	1
GO:0071346	cellular response to interferon-gamma	1.05E-09	0	0	0	1
GO:0071357	cellular response to type I interferon	3.69E-31	0	0	0	1
GO:0098586	cellular response to virus	0.0037813	0	0	0	1
GO:1903900	regulation of viral life cycle	1.50E-18	0	0	0	1
GO:1903901	negative regulation of viral life cycle	1.15E-18	0	0	0	1
GO:1990837	sequence-specific double-stranded DNA binding	0.002945526	0	1	0	0
GO:2001251	negative regulation of chromosome organization	0.039979672	0	1	0	0
REAC:R-HSA-1169408	ISG15 antiviral mechanism	5.61E-12	0	0	0	1
REAC:R-HSA-1169410	Antiviral mechanism by IFN-stimulated genes	5.77E-19	0	0	0	1
REAC:R-HSA-1280215	Cytokine Signaling in Immune system	1.52E-19	0	0	0	1
REAC:R-HSA-168928	DDX58/IFIH1-mediated induction of interferon-alpha/beta	0.001851135	0	0	0	1
REAC:R-HSA-2990846	SUMOylation	0.000289223	0	1	0	0
REAC:R-HSA-3108214	SUMOylation of DNA damage response and repair proteins	0.023406467	0	1	0	0
REAC:R-HSA-	SUMO E3 ligases SUMOylate target proteins	0.000850049	0	1	0	0

3108232						
REAC:R-HSA-3247509	Chromatin modifying enzymes	0.016088428	0	1	0	0
REAC:R-HSA-4839726	Chromatin organization	0.016088428	0	1	0	0
REAC:R-HSA-6806834	Signaling by MET	2.89E-05	0	1	0	0
REAC:R-HSA-877300	Interferon gamma signaling	2.97E-09	0	0	0	1
REAC:R-HSA-8874081	MET activates PTK2 signaling	0.000994797	1	0	0	0
REAC:R-HSA-8934593	Regulation of RUNX1 Expression and Activity	0.000745328	0	1	0	0
REAC:R-HSA-8983711	OAS antiviral response	3.29E-08	0	0	0	1
REAC:R-HSA-9006934	Signaling by Receptor Tyrosine Kinases	0.017643755	0	1	0	0
REAC:R-HSA-909733	Interferon alpha/beta signaling	2.97E-31	0	0	0	1
REAC:R-HSA-913531	Interferon Signaling	4.75E-36	0	0	0	1
REAC:R-HSA-918233	TRAF3-dependent IRF activation pathway	0.000139967	0	0	0	1
REAC:R-HSA-933541	TRAF6 mediated IRF7 activation	0.018776243	0	0	0	1
REAC:R-HSA-936440	Negative regulators of DDX58/IFIH1 signaling	0.000931238	0	0	0	1

Figures

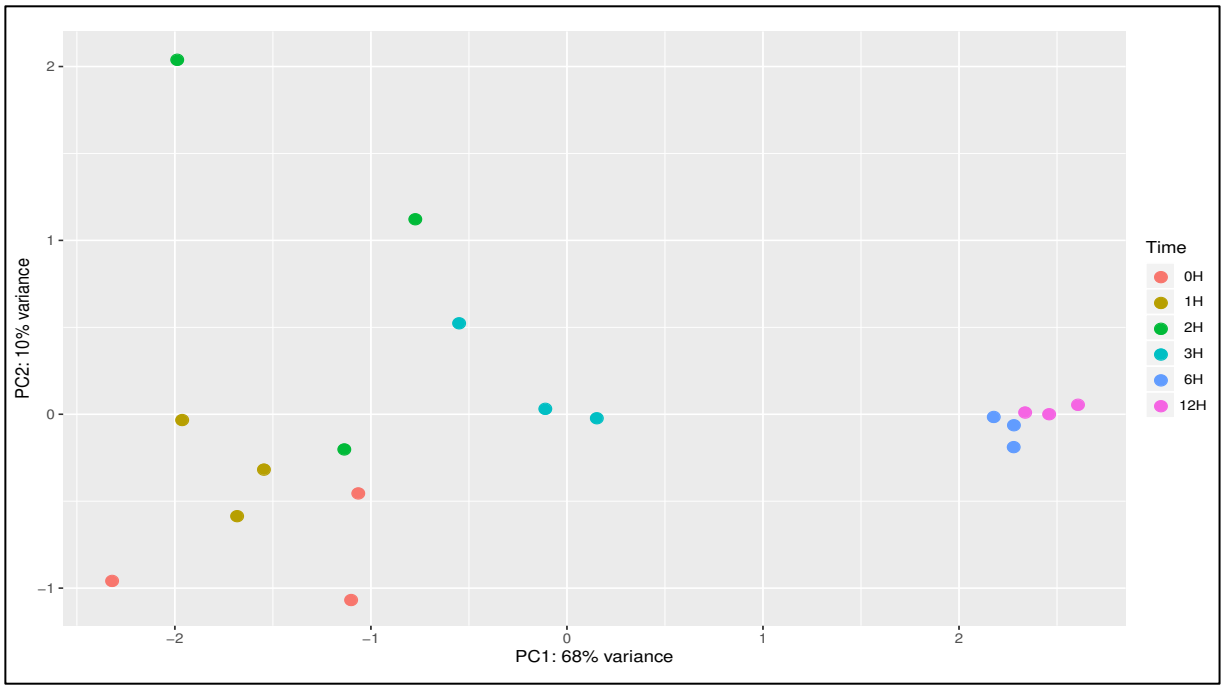

Figure S1. SARS-CoV-2 transcripts clustering. To determine SARS-CoV-2 replication kinetics in human cells using RNA-seq, we infected human lung epithelial cells (Calu-3) at a multiplicity of infection (MOI) of 2. One hour post incubation, virus inoculum was replaced with cell growth media and the clock was set to zero hours. We extracted and sequenced poly-A enriched RNA at 0, 1, 2, 3, 6 and 12 hours post infection (hpi). SARS-CoV-2 genome, sub-genomic RNA and transcripts were detected in infected samples. PCA clustering was performed on quantified SARS-CoV-2 transcript levels in infected samples across time-points. Axes labels indicate the proportion of between-samples variance explained by the first two principal components. H, hours post infection.

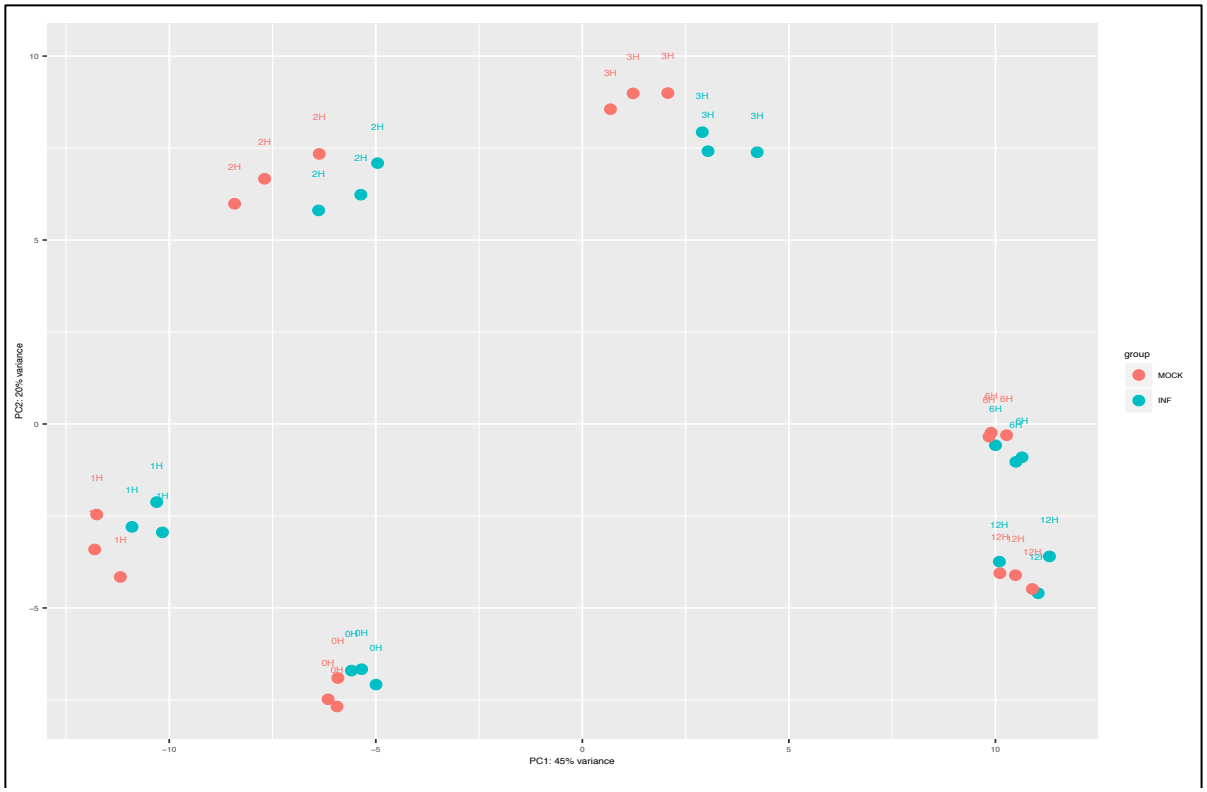

Figure S2. Host-cell transcripts clustering. To determine gene expression in human cells using RNA-seq, we infected human lung epithelial cells (Calu-3) at a multiplicity of infection (MOI) of 2. One hour post incubation, virus inoculum was replaced with cell growth media and the clock was set to zero hours. We extracted and sequenced poly-A enriched RNA at 0, 1, 2, 3, 6 and 12 hours post infection (hpi). PCA clustering was performed on quantified and filtered host gene transcripts in both SARS-CoV-2 infected (blue) and mock infected (red) samples across time-points (indicated in text for each data-point). Axes labels indicate the proportion of between-samples variance explained by the first two principal components. H, hours post infection; Mock, mock infected; INF, SARS-CoV-2 infected.

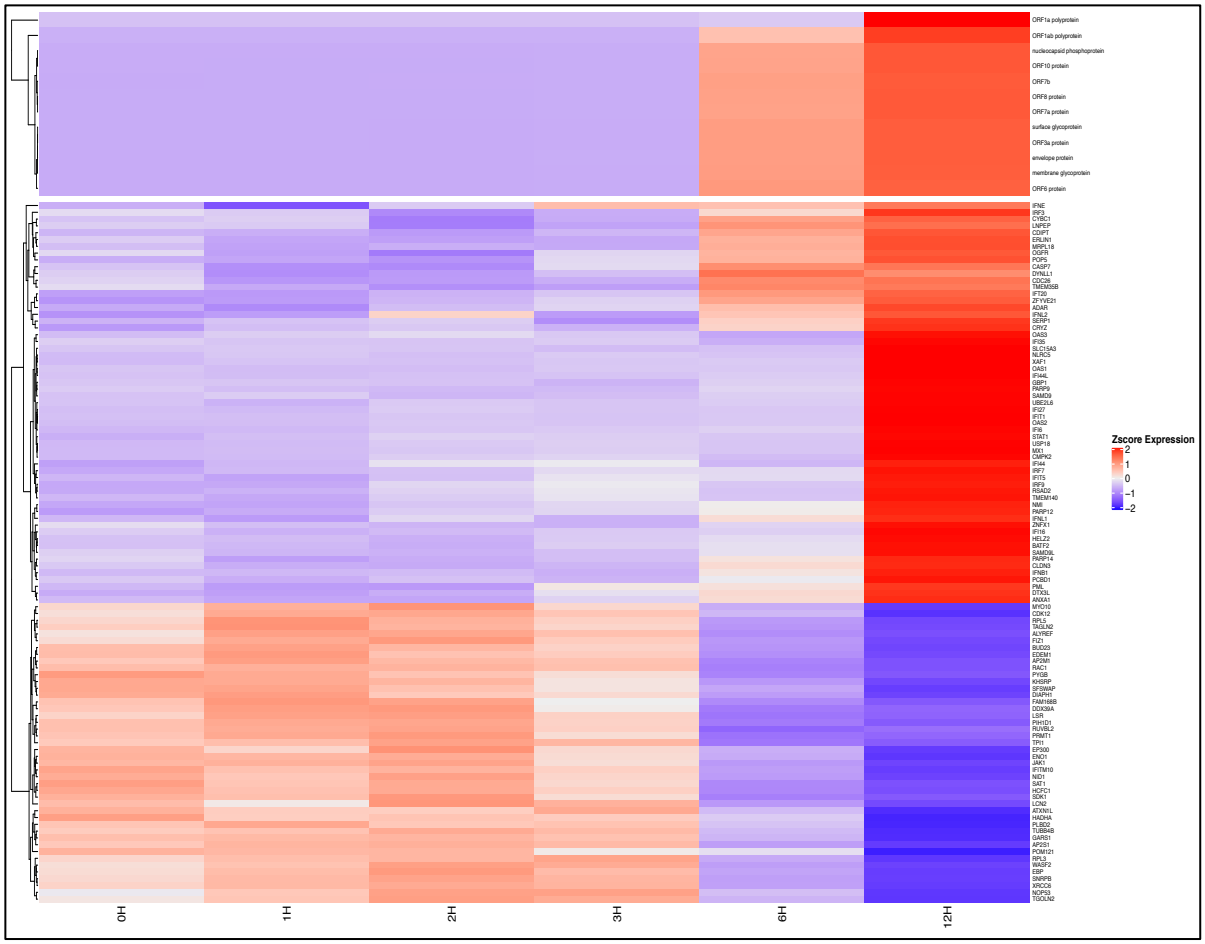

Figure S3. Virus-host correlated transcriptional profiles. Host gene expression that correlated with one or more viral transcripts over the course of infection are shown as z-score normalized expression (bottom), along with viral transcripts (top). Top 100 strongly-correlated genes are represented here. H, hour.

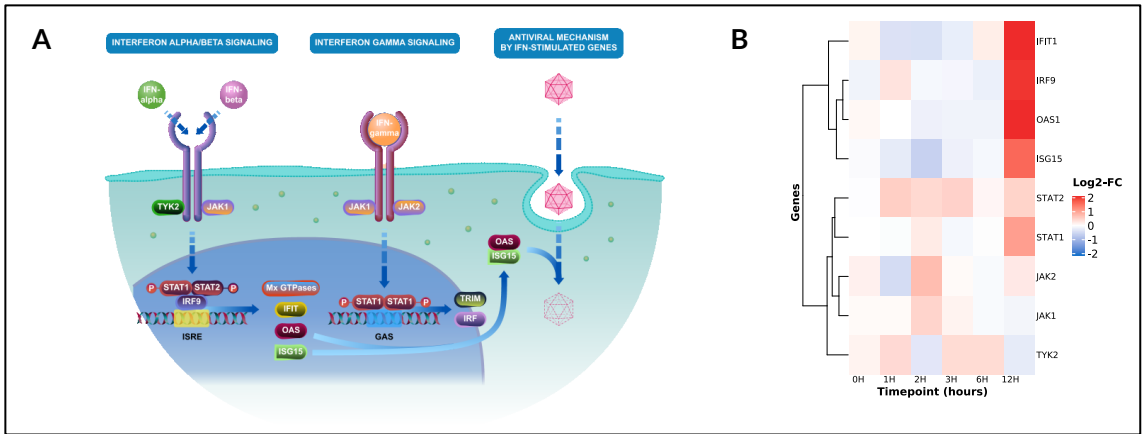

Figure S4. Cytokine signaling in immune system (REAC:R-HSA-1280215). **(A)** Pathway schematic of REACTOME cytokine signalling pathway involving interferon alpha/beta/gamma signalling, and OAS antiviral response mediated by interferon stimulated genes. **(B)** Heatmap of genes within REACTOME cytokine signalling pathway and their $\log_2$ transformed fold-change (FC) between SARS-CoV-2 infected and mock infected samples across all timepoints (0, 1, 2, 3, 6, 12 hrs). H, hours.

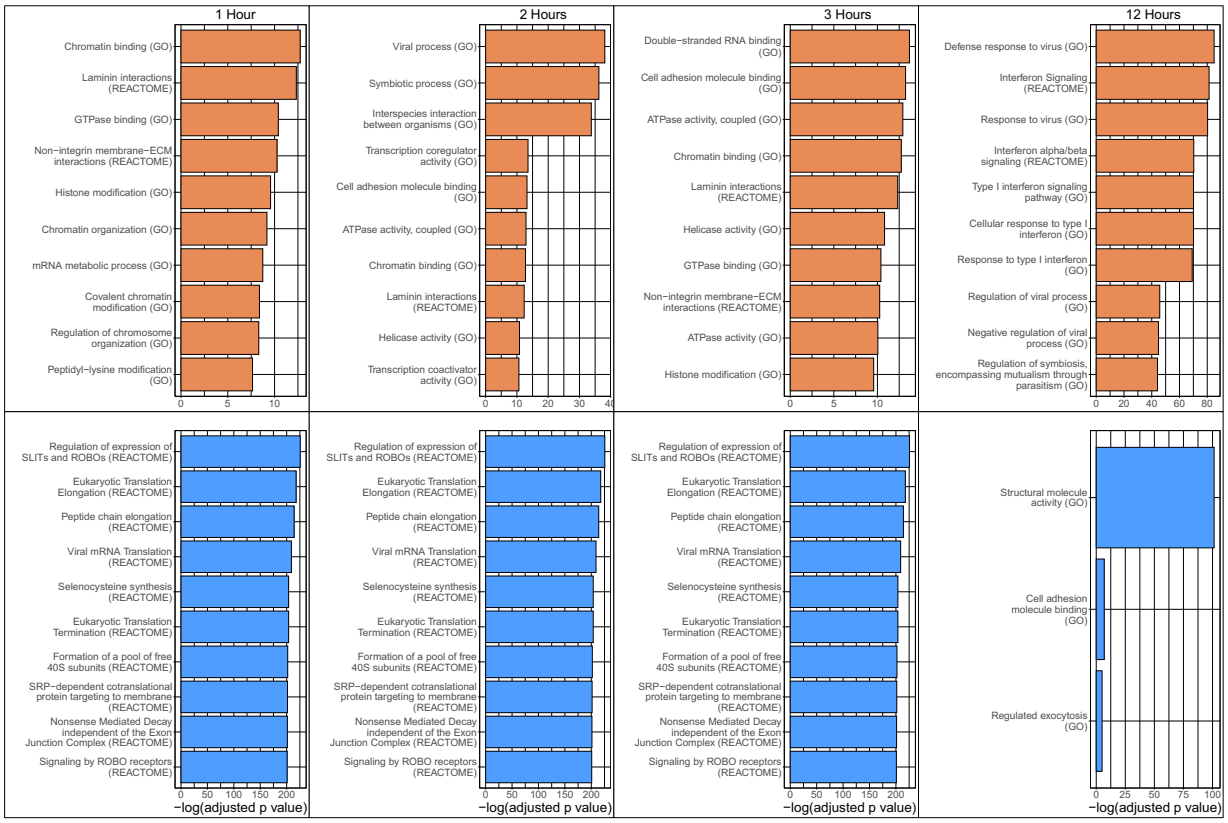

Figure S5. Top functional enrichments over time. Top significantly (adjusted p<0.05) enriched ActivePathway GO terms and REACTOME enrichments for infection vs. mock at 1, 2, 3 and 12 hrs post infection with SARS-CoV-2. Orange bars represent enriched terms associated with genes upregulated in infection vs. mock. Blue bars represent enriched terms associated with genes downregulated in infection vs. mock. 0 and 6 hr time points were omitted due to lack of sufficient numbers of differentially expressed genes.

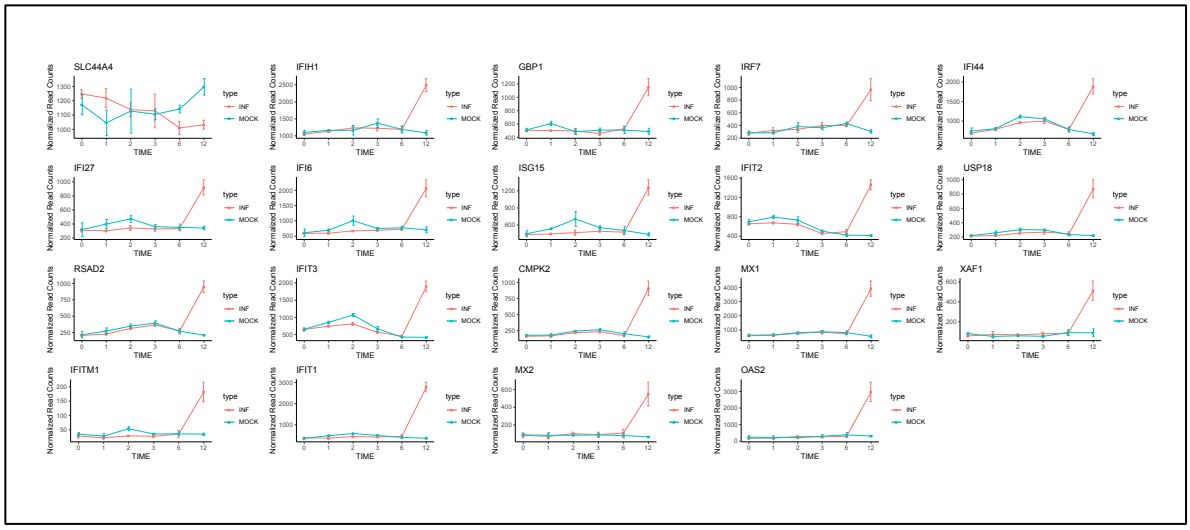

Figure S6. Infection-responsive gene expression profiles for ISGs. ISGs with significantly different levels of transcript expression between mock (blue) and SARS-CoV-2 infected (red) samples at 12 hpi are shown. Normalized read counts per gene, across six time-points are represented here. Time indicated is in hours. Mock, mock infected; INF, SARS-CoV-2 infected.

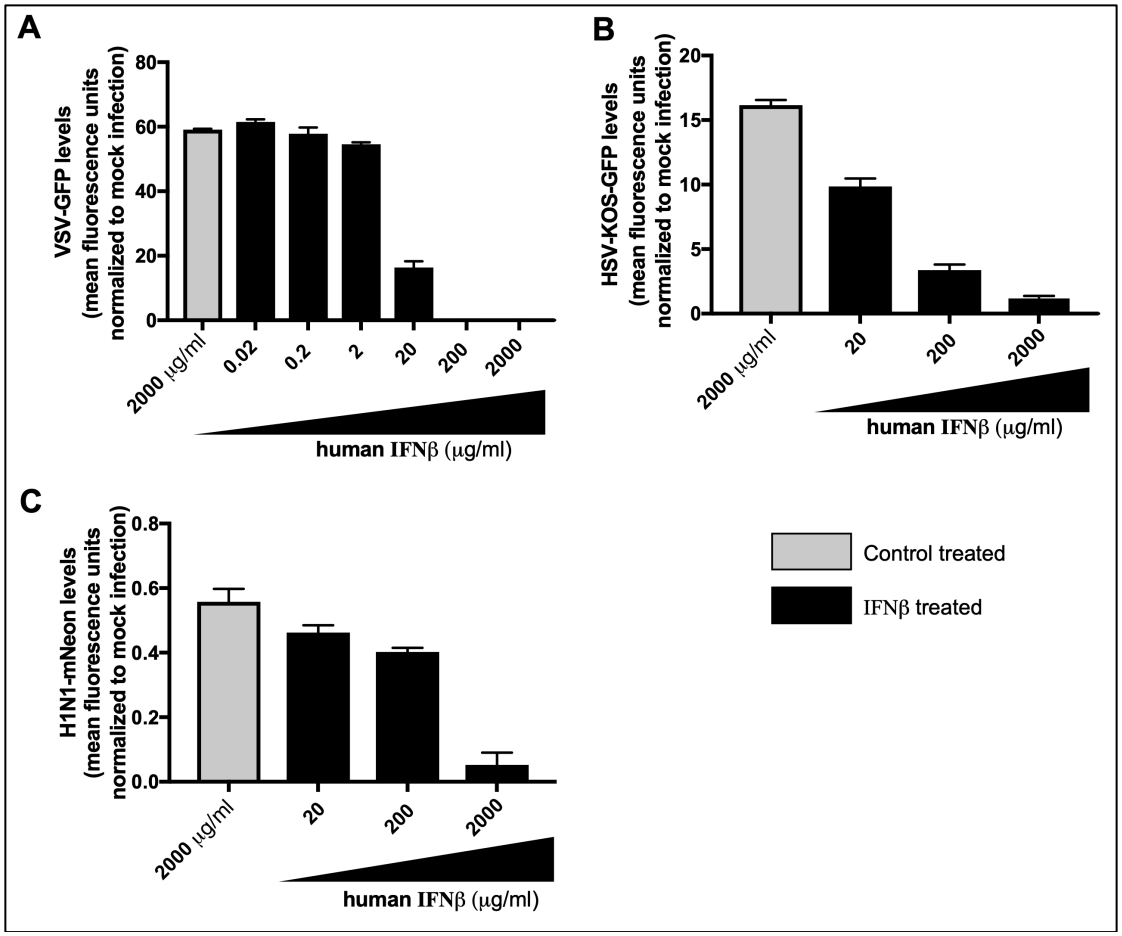

Figure S7. Recombinant human IFNβ1 inhibits VSV, HSV and H1N1 replication. Human fibroblast (THF) cells were treated with increasing concentrations of recombinant human IFNβ1 or mock treated with GFP containing media (control) for 6 hrs. Cells were then infected with vesicular stomatitis virus (VSV-GFP), herpes simplex virus (HSV-KOS-GFP) or H1N1 influenza virus (H1N1-mNeon). VSV and HSV were engineered to express green fluorescent protein (GFP). H1N1 expressed mNeon that is detectable in the same wavelength as GFP. Nineteen hours post infection, GFP/mNeon levels were measured in mock infected and virus infected cells as a surrogate for virus replication. **(A)** VSV-GFP replication in THF cells treated or mock treated with IFNβ1, normalized to mock infection (Mean±SD; n=3). **(B)** HSV-KOS-GFP replication in THF cells treated or mock treated with IFNβ1, normalized to mock infection (Mean±SD; n=3). **(C)** H1N1-mNeon replication in THF cells treated or mock treated with IFNβ1, normalized to mock infection (Mean±SD; n=3).